BIOLOGICAL CRYSTALLOGRAPHY

ISSN 1399-0047

Structures of substrate- and nucleotide-bound propionate kinase from *Salmonella typhimurium*: substrate specificity and phosphate-transfer mechanism

Ambika Mosale Venkatesh Murthy,[a]*‡ Subashini Mathivanan,[a] Sagar Chittori,[a]§ Handanahal Subbarao Savithri[b] and Mathur Ramabhadrashastry Narasimha Murthy[a]

[a]Molecular Biophysics Unit, Indian Institute of Science, Bangalore 560 012, India, and [b]Department of Biochemistry, Indian Institute of Science, Bangalore 560 012, India. *Correspondence e-mail: a.murthy@imb.uq.edu.au

Received 30 March 2015
Accepted 22 May 2015

Edited by R. McKenna, University of Florida, USA

‡ Present address: Institute for Molecular Bioscience, University of Queensland, St Lucia, QLD 4072, Australia.
§ Present address: Laboratory of Cellular and Molecular Neurophysiology, Porter Neuroscience Research Center, NICHD, NIH, DHHS, Bethesda, MD 20892, USA.

Keywords: *St*TdcD; SCFA metabolism; direct in-line phosphate transfer; substrate specificity; kinetic characterization; site-directed mutagenesis.

PDB references: propionate kinase, complex with propionate and AMPPNP, 4xh1; A88V mutant, complex with propionate and AMPPNP, 4xh4; A88G mutant, complex with propionate and AMPPNP, 4xh5

Supporting information: this article has supporting information at journals.iucr.org/d

Kinases are ubiquitous enzymes that are pivotal to many biochemical processes. There are contrasting views on the phosphoryl-transfer mechanism in propionate kinase, an enzyme that reversibly transfers a phosphoryl group from propionyl phosphate to ADP in the final step of non-oxidative catabolism of L-threonine to propionate. Here, X-ray crystal structures of propionate- and nucleotide-bound *Salmonella typhimurium* propionate kinase are reported at 1.8–2.0 Å resolution. Although the mode of nucleotide binding is comparable to those of other members of the ASKHA superfamily, propionate is bound at a distinct site deeper in the hydrophobic pocket defining the active site. The propionate carboxyl is at a distance of ∼5 Å from the γ-phosphate of the nucleotide, supporting a direct in-line transfer mechanism. The phosphoryl-transfer reaction is likely to occur *via* an associative S_N2-like transition state that involves a pentagonal bipyramidal structure with the axial positions occupied by the nucleophile of the substrate and the O atom between the β- and the γ-phosphates, respectively. The proximity of the strictly conserved His175 and Arg236 to the carboxyl group of the propionate and the γ-phosphate of ATP suggests their involvement in catalysis. Moreover, ligand binding does not induce global domain movement as reported in some other members of the ASKHA superfamily. Instead, residues Arg86, Asp143 and Pro116-Leu117-His118 that define the active-site pocket move towards the substrate and expel water molecules from the active site. The role of Ala88, previously proposed to be the residue determining substrate specificity, was examined by determining the crystal structures of the propionate-bound Ala88 mutants A88V and A88G. Kinetic analysis and structural data are consistent with a significant role of Ala88 in substrate-specificity determination. The active-site pocket-defining residues Arg86, Asp143 and the Pro116-Leu117-His118 segment are also likely to contribute to substrate specificity.

1. Introduction

Short-chain fatty acids (SCFAs) such as acetate, propionate and butyrate are abundant in soil and are also found in the human gastrointestinal tract (Cummings *et al.*, 1987). Anaerobic bacterial fermentation of polysaccharides, oligosaccharides, proteins, peptides and glycoprotein precursors in the human gut leads to the production of SCFAs (Cummings & Macfarlane, 1991). SCFAs are extensively used as preservatives in the food industry, as they inhibit bacterial growth (Kabara & Eklund, 1991). Surprisingly, many aerobic bacteria, fungi and anaerobic bacteria such as *Salmonella typhimurium*

Table 1
Oligonucleotides used for the amplification of site-directed mutants of *St*TdcD.

Primer	Sequence† (5′–3′)	Remarks
A88G, sense	ATTG**GACACC**GTATC*GGG*CACGGTGGAGAGTTA	ΔBstEII‡
A88G, antisense	TAACTCTCCACCGTG*CCC*GATAC**GGTGTC**CAAT	
A88V, sense	ATTG**GACACC**GTATC*GTG*CACGGTGGAGAGTTA	ΔBstEII‡
A88V, antisense	TAACTCTCCACCGTG*CAC*GATAC**GGTGTC**CAAT	

† The desired site of mutation is shown in italics. ‡ The restriction site was deleted in the mutants.

and *Escherichia coli* are able to use SCFAs as a source of carbon and energy (Horswill & Escalante-Semerena, 1999; Klein *et al.*, 1971).

SCFA metabolism is vital for the virulence and survival of *Salmonella*. In *E. coli* and *S. typhimurium*, the anaerobically regulated *tdc* (*tdcABCDEFG*) operon encodes the enzymes necessary for the degradation of L-serine and L-threonine to acetate and propionate, respectively (Hesslinger *et al.*, 1998; Sawers, 2001, 1998; Simanshu *et al.*, 2007). Propionate kinase (TdcD) catalyzes the final step in the catabolism of L-threonine to propionate by facilitating the reversible transfer of phosphate from propionyl phosphate to ADP, leading to the formation of propionate and ATP (Hesslinger *et al.*, 1998). TdcD is a homodimeric enzyme and shares significant sequence identity (38–44%) with the well studied acetate kinases (Buss *et al.*, 2001; Chittori *et al.*, 2012; Fox & Roseman, 1986; Gorrell *et al.*, 2005). Each monomer of TdcD is comprised of two domains (domains I and II). Each domain consists of a core secondary structure $\beta\beta\beta\alpha\beta\alpha\beta\alpha$, similar to the fold found in proteins belonging to the acetate and sugar kinase/heat-shock cognate (Hsc) 70/actin (ASKHA) superfamily (Bork *et al.*, 1992). In all of these enzymes the active site is at the interdomain cleft (Hurley, 1996). In acetate kinase, the two domains close around the active-site pocket after substrate binding (Buss *et al.*, 2001; Bork *et al.*, 1992; Bennett & Steitz, 1978). Two different catalytic mechanisms have been suggested based on studies of *E. coli* acetate kinase: direct in-line transfer of the phosphoryl group of ATP to acetate (Blättler & Knowles, 1979) or a covalent triple-displacement mechanism requiring two phosphoenzyme intermediates (Spector, 1980). In spite of the overall structural similarity and the conservation of active-site residues, *S. typhimurium* acetate and propionate kinases have distinct substrate specificities for acetate and propionate, respectively. However, apart from the preferred substrate, these enzymes can utilize alternative SCFAs with lower catalytic rates. They also exhibit broad specificity with respect to nucleotides (purines and pyrimidines; Gorrell *et al.*, 2005; Chittori *et al.*, 2013)

We have previously reported biochemical characterization of *S. typhimurium* TdcD (*St*TdcD) and its crystal structure in the unliganded state, as well as in complexes with AMP, ATP, ADP, GMP, GTP, GDP, CTP, CMP, the nonhydrolyzable ATP analogue AMPPNP and AP4A (Simanshu *et al.*, 2005, 2008; Chittori *et al.*, 2013). However, crystals of substrate-bound *St*TdcD could not be obtained. Here, we report the structure of propionate- and AMPPNP-bound wild-type *St*TdcD as well as of the active-site mutants A88V and A88G. Comparative analysis of the present and previously determined structures shows that there is no domain movement upon ligand binding, unlike in some other ASKHA family members. The present structures reveal propionate binding to a site closer to the γ-phosphate of AMPPNP compared with that observed in the substrate-bound structures of acetate kinase (Gorrell *et al.*, 2005), supporting the direct in-line phosphoryl-transfer mechanism of catalysis. Ligand binding in propionate kinase is accompanied by side-chain movement of His118, Arg86, Asp143 and the Pro116-Leu117-His118 segment towards the substrate, leading to the expulsion of water molecules from the active site. The present structural and kinetic studies of the mutants support the previously proposed inverse correlation between the bulk of the side chain of the residue corresponding to Ala88 of *St*TdcD and SCFA specificity.

2. Materials and methods

2.1. Site-directed mutagenesis

Site-directed mutants were obtained by a PCR-based method (Weiner & Costa, 1994) using a recombinant plasmid containing the TdcD gene cloned into pRSETC (Invitrogen) as the template. PCR was carried out using the primers indicated in Table 1. The PCR reaction mixture was treated with DpnI enzyme at 37°C for 1 h to digest the methylated template DNA and the resulting mixture was transformed into *E. coli* DH5α cells. Plasmids from a single colony were isolated and the presence of the mutant gene was screened by restriction digestion and confirmed by DNA sequencing (Table 1).

2.2. Protein purification

Wild-type and mutant *St*TdcDs were overexpressed in *E. coli* BL21 pLysS cells and purified as described previously (Simanshu *et al.*, 2005). The purity and homogeneity of the wild-type and mutant proteins were examined by SDS–PAGE and size-exclusion chromatography. The protein concentration was determined by the method of Bradford (1976) using a NanoDrop spectrophotometer. The mutant proteins behaved in a manner similar to the wild type in terms of solubility and yield (10–15 mg per litre of *E. coli* culture).

2.3. Enzymatic assays

The enzymatic activity of wild-type and mutant *St*TdcD was estimated by a coupled spectrophotometric assay. The reaction was monitored by coupling the ADP produced to the oxidation of NADH by pyruvate kinase and lactate dehydrogenase (LDH; Simanshu *et al.*, 2005). The 1.0 ml reaction mixture of consisted of 50 m*M* HEPES–NaOH pH 7.5, 25 m*M* propionate, 1 m*M* ATP, 1.5 m*M* $MgCl_2$, 5 m*M* phosphoenolpyruvate, 0.25 m*M* NADH, 15 units of pyruvate kinase and 20 units of LDH. The reaction was started by the addition of

Table 2
Data-collection and refinement statistics for ligand-bound wild-type and mutant *St*TdcDs.

Values in parentheses are for the highest resolution shell.

	*St*TdcD–propionate–AMPPNP	A88G *St*TdcD–propionate–AMPPNP	A88V *St*TdcD–propionate–AMPPNP
Crystallization condition	0.1 *M* bis-tris pH 6.5, 20% polyethylene glycol monomethyl ether 5000	0.1 *M* bis-tris pH 6.5, 30% pentaerythritol ethoxylate, 0.05 *M* ammonium sulfate	0.1 *M* bis-tris pH 6.5, 30% pentaerythritol ethoxylate, 0.05 *M* ammonium sulfate
Resolution range (Å)	32.22–2.00 (2.11–2.00)	42.59–2.11 (2.23–2.11)	32.03–1.80 (1.90–1.80)
Space group	$P3_121$	$P3_121$	$P3_121$
Unit-cell parameters (Å)	$a = b = 111.61$, $c = 66.5$	$a = b = 110.96$, $c = 66.44$	$a = b = 110.96$, $c = 66.44$
No. of observed reflections	238548	148147	200990
No. of unique reflections	32233	27037	42396
Multiplicity	7.4	5.5	4.7
Completeness (%)	99.0 (98.5)	97.8 (92.4)	96.9 (95.6)
$\langle I/\sigma(I)\rangle$†	17.0 (4.0)	9.5 (3.2)	17.5 (2.7)
$R_{\rm merge}$‡ (%)	7.1 (50.7)	10.0 (50.1)	4.7 (48.1)
Matthews coefficient (Å^3 Da^{-1})	2.72	2.69	2.68
Solvent content (%)	55.32	55.52	54.18
Refinement statistics			
$R_{\rm work}/R_{\rm free}$§ (%)	18.06/22.57	16.69/22.56	18.47/22.48
No. of atoms			
Protein	2923	2917	2933
Water	112	105	135
Ligand	36	36	36
Others	12	6	6
Average *B* factor (Å^2)			
Protein	35.68	39.19	33.43
Water	42.26	38.06	38.45
Ligand	48.33	55.00	45.71
Others	43.58	35.01	38.24
Ligand occupancy	0.7	0.7	0.7
R.m.s. deviations			
Bond lengths (Å)	0.019	0.016	0.019
Bond angles (°)	1.95	1.85	1.97
Dihedral angles (°)	6.67	6.60	6.60
Chiral-centre restraints (Å^3)	0.116	0.105	0.128
General planes (Å)	0.009	0.008	0.010
Ramachandran plot (%)			
Most favoured	92.1	90.9	91.6
Additionally allowed	7.0	8.8	8.1
Generously allowed	0.9	0.3	0.0
Disallowed	0.3	0.0	0.3

† I is the integrated intensity and $\sigma(I)$ is the estimated standard deviation of that intensity. ‡ $R_{\rm merge} = \sum_{hkl}\sum_i |I_i(hkl) - \langle I(hkl)\rangle|/\sum_{hkl}\sum_i I_i(hkl)$, where $I_i(hkl)$ is the ith measurement of the intensity of reflection hkl and $\langle I(hkl)\rangle$ is the mean intensity. § $R_{\rm work} = \sum_{hkl} \big||F_{\rm obs}| - |F_{\rm calc}|\big|/\sum_{hkl}|F_{\rm obs}|$; $R_{\rm free}$ was calculated using 5% of the reflections, which were excluded from the refinement.

propionate kinase or its mutants and progress was monitored at 37°C by the reduction in absorbance at 340 nm owing to the disappearance of NADH. Enzymatic activity for the utilization of acetate and butyrate as substrates was also monitored in a similar manner. To deduce kinetic parameters for SCFAs, 25 m*M* $MgCl_2$ and 5 m*M* ATP were maintained in excess, whereas to determine kinetic constants for ATP, 25 m*M* $MgCl_2$ and 50 m*M* propionate were maintained in excess. All enzyme assays were repeated three times from independent purifications. Kinetic parameters were evaluated by fitting the initial velocity *versus* the substrate concentration to the Michaelis–Menten equation using the nonlinear regression analysis option in *GraphPad Prism* 6 (GraphPad Software, California, USA).

2.4. Crystallization and data collection

Wild-type and mutant *St*TdcD were concentrated to 30 mg ml^{-1} using Amicon Ultra-15 centrifugal filter units (EMD Millipore, Massachusetts, USA). Protein–ligand complexes were obtained by overnight incubation of the respective proteins (10 mg ml^{-1}) with 10 m*M* AMPPNP and 10 m*M* propionate at 4°C. Crystals of *St*TdcD complexes were obtained using the hanging-drop method under similar conditions to those used previously for unliganded *St*TdcD (Simanshu *et al.*, 2005). Crystals were cryoprotected with 20% glycerol prior to data collection (Supplementary Fig. S1 and Table 2). These crystals diffracted to 1.8–2.1 Å resolution and a complete data set was collected at the EMBL synchrotron facility, Grenoble, France. All data sets were processed using *iMosflm* 1.0.7 and *SCALA* from the *CCP*4 suite of programs (Winn *et al.*, 2011). Initial phases of reflections were obtained by molecular replacement (MR) using *Phaser* (McCoy *et al.*, 2007) and a polyalanine model of the apo *St*TdcD protomer (PDB entry 2e1y; Simanshu *et al.*, 2005) as the phasing model. The initial models obtained by MR were further improved by alternative rounds of manual model building using *Coot* (Emsley & Cowtan, 2004) and refinement using *REFMAC*5

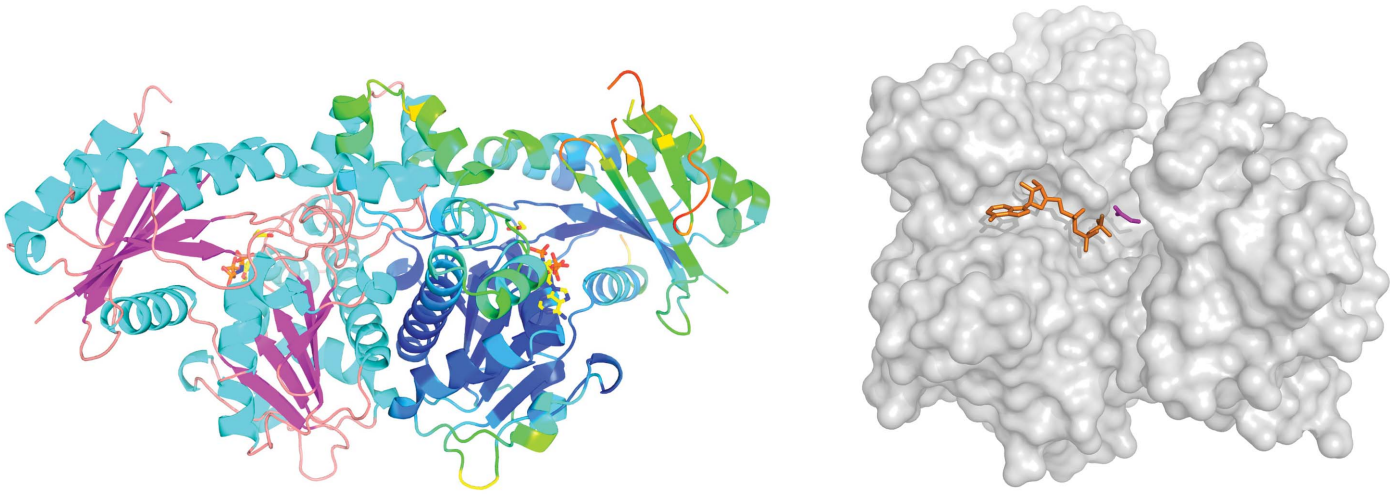

(*a*) (*b*)

Figure 1
Crystal structure of ligand-bound TdcD. (*a*) Cartoon diagram of homodimeric *St*TdcD in complex with propionate and AMPPNP. The subunit on the left shows α-helices in teal and β-strands in pink. *B*-factors were used to colour the subunit on the right (rainbow colouring with violet representing the lowest and red representing the highest *B* factors). Propionate and AMPPNP are represented as ball-and-stick models. (*b*) Surface representation of an *St*TdcD–propionate–AMPPNP monomer portraying propionate (magenta) and AMPPNP (orange) binding in the interdomain cleft. Surface transparency is set to 50% and ligands are represented as ball-and-stick models.

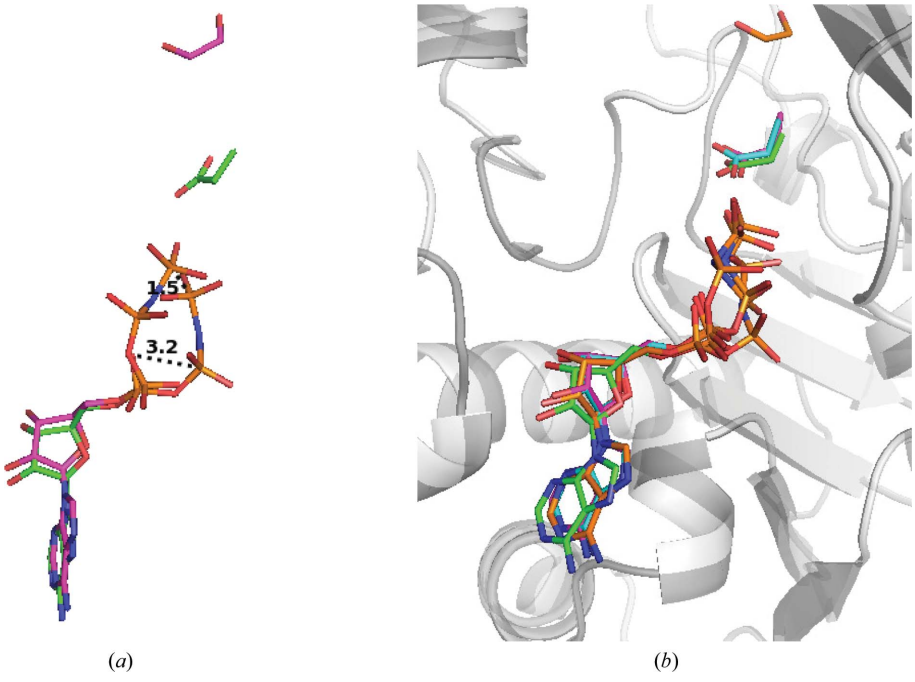

(*a*) (*b*)

Figure 2
Superposition of ternary complexes of *St*TdcD and its mutants on AMPPNP-bound *St*TdcD, illustrating changes in the mode of nucleotide binding. (*a*) Superposition of propionate/AMPPNP-bound *St*TdcD (C atoms in green) on EDO/AMPPNP-bound *St*TdcD (C atoms in magenta). It was previously assumed that the EDO in EDO–AMPPNP–*St*TdcD represents the substrate-binding site. (*b*) Superposition of ternary complexes of wild-type (C atoms in green), A88G (C atoms in cyan) and A88V (C atoms in magenta) *St*TdcD on EDO/AMPPNP-bound wild-type *St*TdcD (C atoms in orange). The background secondary structure represented in grey corresponds to the *St*TdcD ternary complex.

(Murshudov *et al.*, 2011). Coordinates and structure-factor files have been deposited in the Protein Data Bank with the following accession codes: propionate/AMPPNP-bound *St*TdcD, 4xh1; A88G *St*TdcD, 4xh5; A88V *St*TdcD, 4xh4.

3. Results

3.1. Structures of ternary complexes of wild-type and mutant *St*TdcD

The polypeptide folds of the *St*TdcD–propionate–AMPPNP and the mutant *St*TdcD–propionate–AMPPNP complexes are very similar to that of native *St*TdcD, consisting of two domains. Each domain has a core $\beta\beta\beta\alpha\beta\alpha\beta\alpha$ secondary structure similar to those of acetate kinase/glycerol kinase/hexokinase/Hsc70/actin (Fig. 1*a*). Superposition of all C^{α} atoms of propionate-bound *St*TdcD–AMPPNP and *St*TdcD–AMPPNP (PDB entry 1x3n; Simanshu *et al.*, 2005) results in an r.m.s. deviation of 0.42 Å, suggesting that there are no large-scale conformational changes upon the binding of propionate. Similarly, superposition of the propionate-bound A88G *St*TdcD–AMPPNP and A88V *St*TdcD–AMPPNP structures with *St*TdcD–AMPPNP resulted in r.m.s.d.s of ∼0.32 Å, indicating that no substantial change in conformation had occurred owing to the mutation of the Ala88 residue. As anticipated, the nucleotide and substrate are bound in the cleft between the two domains (Fig. 1*b*). As in the wild-type structure, electron density was poor for residues 39–42 and 49–58.

3.2. Mode of nucleotide binding

In the propionate-bound wild-type and Ala88 mutant *St*TdcD crystal structures, the adenine ring and ribose are positioned in a similar manner as in *St*TdcD–AMPPNP (Simanshu *et al.*, 2005). The adenine ring is in an *anti* confirmation with respect to the ribose sugar, and the sugar ring is in the C2′-*endo* form with its O5′ atom in the *trans*, *gauche* confirmation. In contrast, the interactions of the α-phosphate O atoms with protein atoms are different. One of the O atoms is hydrogen-bonded to the main-chain N atom of Asn206. Also, there is a pronounced difference in the positioning of the β- and γ-phosphates of AMPPNP (Fig. 2*a*). Thus, the phosphate positions are influenced by substrate binding. Concurrently, shifts in the position of several active-site residues are observed.

In the propionate-bound *St*TdcD–AMPPNP ternary complex, the β-phosphate position is shifted by 3.4 Å towards Gly325 when compared with the *St*TdcD–AMPPNP complex (Simanshu *et al.*, 2005), while the displacement of the γ-phosphate is only 1.5 Å. The displacement of the β-phosphate could be owing to steric hindrance from the Asn206 side chain, the conformation of which is different in the wild-type and the ternary-complex structures. One of the β-phosphate O atoms forms a hydrogen bond to a water molecule and the main-chain N atom of Gly326. The γ-phosphate O atoms are hydrogen-bonded to His175 and the main-chain N atom of Gly207. These interactions are different from those of the wild-type enzyme and hence are owing to structural changes brought about by substrate binding. In the A88V and A88G mutant *St*TdcD structures bound to propionate and AMPPNP, the β-phosphate is less displaced (2.5 and 2.9 Å, respectively) relative to wild-type *St*TdcD–AMPPNP (Fig. 2*b*) and the side chain of Asn206 is less perturbed. However, the phosphate O atoms are bound as in the *St*TdcD–propionate–AMPPNP structure (Supplementary Figs. S3*b* and S4*b*).

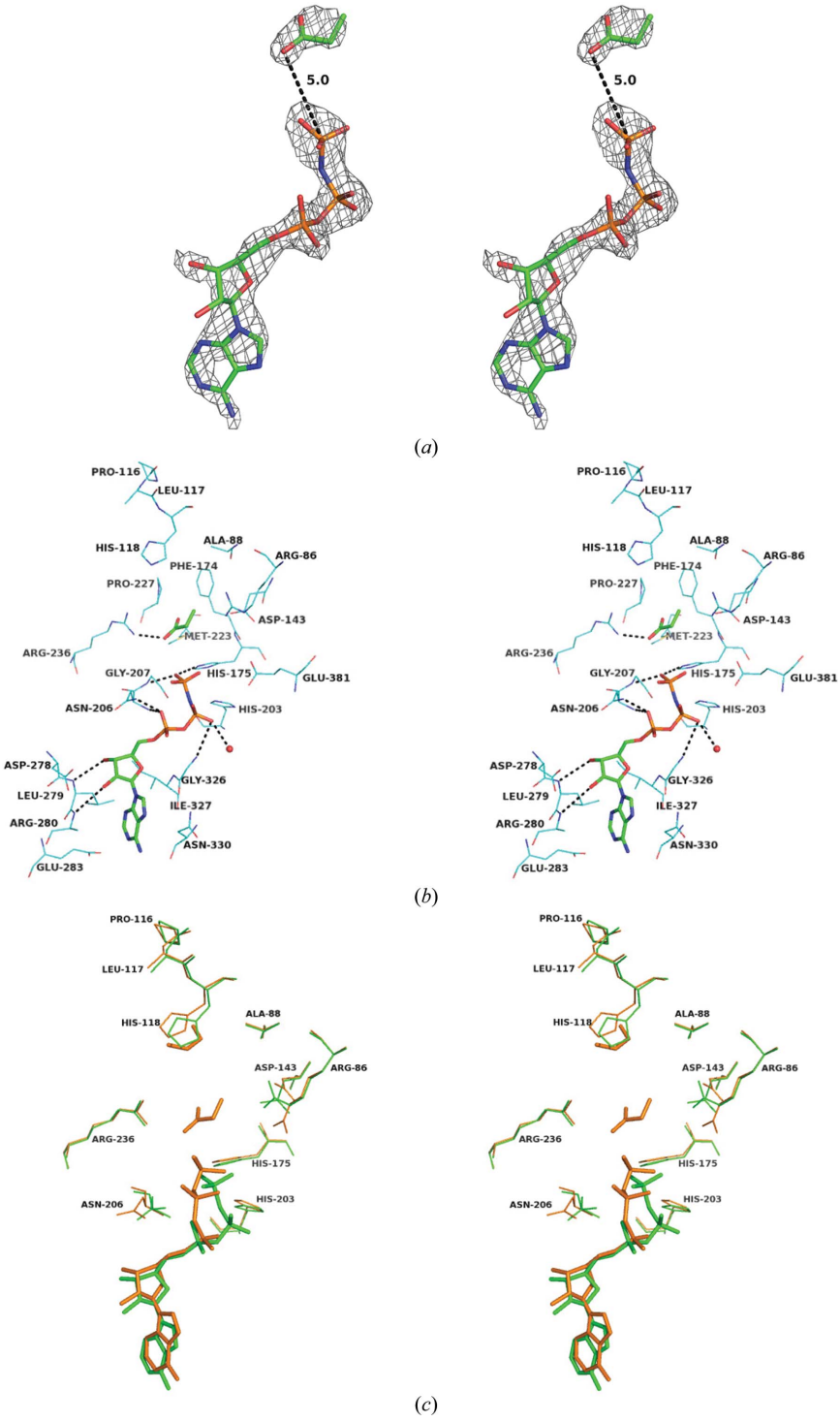

Figure 3
Ligand binding in the *St*TdcD–AMPPNP complex. (*a*) Stereoview of the electron density corresponding to AMPPNP and propionate from a $2F_o - F_c$ map contoured at 1.0σ. (*b*) Stereo diagram of the active-site pocket showing interactions with the nucleotide and bound propionate. Hydrogen bonds are indicated by broken grey lines, whereas AMPPNP and propionate are shown as ball-and-stick models. (*c*) Stereo illustration of structural superposition of the nucleotide and the neighbouring interacting residues of *St*TdcD–propionate–AMPPNP (green) and *St*TdcD–AMPPNP (orange).

3.3. Propionate-binding site

In the crystal structure of the *St*TdcD–AMPPNP complex, the cryoprotectant EDO was bound in a hydrophobic pocket close to that of bound AlF_3 in acetate kinase (Figs. 2*a* and Supplementary Fig. S2). This site, lined by His118, His175, Arg86 and Arg236, which are conserved in *Thermotoga maritima* butyrate kinase 2 (*Tm*Buk2; Diao & Hasson, 2009) and *Methanosarcina thermophila* acetate kinase (*Mt*AckA; Gorrell *et*

al., 2005), was assumed to form the substrate-binding pocket (Supplementary Fig. S2). Val93 in AckA, which is close to the hydrophobic pocket, is substituted by Ala88 in *St*TdcD and Gly76 in butyrate kinase. The substitutions appeared to correlate with the volumes of the respective substrates. Therefore, it was proposed that Val, Ala and Gly were the specificity-determining residues in AckA, TdcD and Buk2, respectively (Chittori *et al.*, 2013).

In the present study, a clear Y-shaped density near to the γ-phosphate is observed for propionate in both the wild-type and the Ala88 mutant structures crystallized in the presence of propionate and AMPPNP (Fig. 3*a*, Supplementary Figs. S3*a* and S4*a*). This site is distinct from the EDO binding site in the *St*TdcD–AMPPNP complex as the propionate is bound closer to the nucleotide in the present structures. One of the O atoms of the propionate carboxylate is at a distance of 5 Å from the γ-phosphate of AMPPNP. The geometry is suitable for direct in-line transfer of a phosphate group from the nucleotide to the substrate (Fig. 3*b*). The propionate is surrounded by conserved residues such as Pro227, His118, Arg86, Glu381, Ala88, Arg236, His175, Met223 and Asp143. The O atom of the propionate forms a hydrogen bond to the conserved Arg236 residue. The hydrocarbon end of the propionate points towards Ala88 and is held by the hydrophobic pocket formed by the conserved Ala88, Pro227, Phe174 and the side chain of Arg86. Substrate binding is accompanied by displacement of the side chains of these conserved residues (Fig. 3*c*). In comparison with the *St*TdcD–AMPPNP structure, the Pro116-Leu117-His118 segment moves towards the substrate, and His118, the side chain of Arg86 and Asp143 move by 1.1, 1.8 and 1.5 Å, respectively. Thus, the movement of these conserved residues determines the size of the active-site pocket. Although EDO was bound at a distance of ∼5 Å from the γ-phosphate of ATP and GTP in the SCFA II site proposed in our previous studies (Chittori *et al.*, 2013), no rearrangement of phosphate moieties or displacement of residues lining the active pocket was apparent as evident in our current studies.

In the structures of the ternary complexes of the *St*TdcD Ala88 mutants, the propionate is at a distance of ∼4 Å from the γ-phosphate of AMPPNP and is surrounded by the same conserved residues as in the *St*TdcD–propionate–AMPPNP complex (Supplementary Figs. S3*b* and S4*b*). When the A88G *St*TdcD–propionate–AMPPNP structure was superposed on *St*TdcD–AMPPNP (Supplementary Fig. S3*c*), a slight movement of Arg86 by 0.5 Å towards the substrate and an outward movement of His118 by ∼1 Å was observed. In contrast, when A88V *St*TdcD–propionate–AMPPNP was superposed on *St*TdcD–AMPPNP (Supplementary Fig. S4*c*), a larger movement of His118 and Arg86 of ∼1.7 and 1.4 Å, respectively, towards the substrate in addition to an inward movement of the Glu381 side chain by ∼1.2 Å was observed.

3.4. Kinetic analysis of wild-type and mutant *St*TdcDs

Kinetic constants for the wild-type and mutant *St*TdcDs are listed in Table 3. The K_m and k_{cat} for ATP are similar for the wild-type and mutant *St*TdcDs. However, K_m for propionate is higher by twofold and sixfold for A88V *St*TdcD and A88G *St*TdcD, respectively, compared with the wild-type enzyme. Also, the K_m of A88G *St*TdcD for butyrate is lower by fivefold and fourfold relative to the wild-type enzyme and A88V *St*TdcD, respectively. Likewise, K_m for acetate of A88V *St*TdcD is lower by twofold and 24-fold compared with wild-type and A88G *St*TdcD, respectively. These K_m data suggest that wild-type, A88G and A88V *St*TdcDs have a higher affinity for propionate, butyrate and acetate, respectively. In addition, k_{cat}/K_m for propionate is five times and 1.4 times greater for the wild type relative to the A88G and A88V mutants, respectively. Tenfold and 33-fold increases in the k_{cat}/K_m values for acetate were observed for the A88V mutant with respect to the wild type and the A88G mutant, respectively. A88V *St*TdcD showed about a fivefold and a 47-fold increase in k_{cat}/K_m for butyrate compared with wild-type and A88G *St*TdcD, respectively. These observations confirm that the preferred substrates of the wild type and the A88G and A88V mutants are propionate, butyrate and acetate, respectively. These results further confirm that the substrate-specificity determinant is indeed the amino acid at the position equivalent to residue 88 of *St*TdcD.

Table 3
Kinetic parameters determined for wild-type and mutants of *St*TdcD.

Values recorded indicate the mean ± standard deviation from three independent experiments.

	K_m (m*M*)	V_{max} (µmol mol^{-1} mg^{-1})	k_{cat} (s^{-1})	k_{cat}/K_m (m*M*$^{-1}$ s^{-1})
Acetate				
Wild type	25 ± 2	150 ± 17	120 ± 15	4.0 ± 1.0
A88G	56 ± 2	98 ± 9	75 ± 10	1.3 ± 0.2
A88V	2.3 ± 0.8	160 ± 18	102 ± 17	44.3 ± 3.6
Propionate				
Wild type	2.5 ± 0.2	150 ± 15	105 ± 14	42.0 ± 4.8
A88G	16 ± 0.8	187 ± 7	141 ± 9	8.8 ± 2.8
A88V	4.5 ± 0.22	190 ± 16	144 ± 17	32.0 ± 3.2
Butyrate				
Wild type	32 ± 4	78 ± 10	60 ± 10	1.8 ± 1.0
A88G	7.6 ± 0.9	78 ± 8	59 ± 7	7.7 ± 1.6
A88V	27.3 ± 2	7 ± 1	4 ± 0.5	0.17 ± 0.02
ATP				
Wild type	0.126 ± 0.015	150 ± 10	120 ± 17	952.38 ± 20
A88G	0.132 ± 0.023	145 ± 25	110 ± 20	833.33 ± 10
A88V	0.129 ± 0.021	180 ± 20	136 ± 16	1054 ± 30

3.5. Plausible catalytic mechanism

As depicted in Fig. 3(*b*), propionate is secured in a hydrophobic pocket formed by Ala88, Pro227, Met223 and Phe174. The carboxyl group of the propionate forms a hydrogen bond to Arg236. After propionate binding, the γ-phosphate of the nucleotide is positioned at an appropriate distance (∼4–5 Å) from the carboxylate of the substrate. Therefore, phosphoryl transfer might follow an S_N2 associative mechanism initiated by nucleophilic attack by the carboxyl group of propionate on the γ-phosphate of the nucleotide (Fig. 6). A pentacoordinate transition state may be attained with the carboxyl group of the substrate and the O atom bridging the β- and γ-phosphates

of the nucleotide at axial positions and three oxyanions at equatorial positions. A magnesium ion, Arg236, His175 and His203 might stabilize the oxyanions of the transition state. After propionyl phosphate is formed, the products can be released from the active site and the enzyme is ready for the next cycle of reaction. Superposition of monomer *B* of acetate kinase from *M. thermophila* on ligand-bound *St*TdcD suggests that the AlF_3 transition-state analogue is similar to the proposed pentacoordinate transition state, further supporting the proposed catalytic mechanism (Fig. 4).

4. Discussion

Acetate, propionate and butyrate, which are the metabolic products of fermentation, constitute 80% of the SCFAs in the human gut (Cummings & Macfarlane, 1991; Sears, 2005). The survival and pathogenicity of *S. typhimurium* is impaired by SCFAs, which interfere with many cellular processes (Blankenhorn *et al.*, 1999; Salmond *et al.*, 1984). Surprisingly, *E. coli* and *S. typhimurium* have been shown to evade SCFA toxicity and to utilize them as a source of energy and carbon (Cummings *et al.*, 1987; Horswill & Escalante-Semerena, 1999). Therefore, understanding the metabolism of SCFAs in *S. typhimurium* is of great interest. We have previously reported the structure and function of propionate kinase, acetate kinase, methyl isocitrate lyase, threonine deaminase and methyl citrate synthase involved in SCFA metabolism (Simanshu *et al.*, 2003, 2005; Chittori *et al.*, 2011). It was found that TdcD could utilize not only propionate but also acetate and butyrate as substrates (Chittori *et al.*, 2013). In addition, it was hypothesized that TCA-cycle intermediates such as citrate, succinate, 2-ketobutyrate, α-ketoglutarate and malate might inhibit *St*TdcD activity (Chittori *et al.*, 2013).

Several attempts have previously been made to obtain the structure of ligand-bound *St*TdcD with the aim of understanding substrate-induced conformational changes and the mechanism of catalysis. However, these studies were not successful. In the present studies, we obtained the first *St*TdcD–propionate–AMPPNP ternary complex using glycerol as the cryoprotectant in order to avoid the binding of EDO to the active site. Propionate was bound at a distance of 5 Å from the γ-phosphate of AMPPNP. Although the adenine ring and sugar are sandwiched by hydrophobic interactions, as observed in the unliganded form, the arrangement of the phosphate atoms is profoundly altered. Unlike in some other members of the acetokinase family of enzymes, no large conformational changes were observed upon ligand binding (Bennett & Steitz, 1978; Schnick *et al.*, 2009; van den Ent *et al.*, 2002; Gorrell & Ferry, 2007). However, ligand binding is associated with local structural changes such as movement of the Pro116-Leu117-His118 segment and movement of the side chains of residues lining the active-site pocket towards the substrate. From previous studies it was postulated that Ala88 is the substrate-specificity determining residue (Simanshu *et al.*, 2005). Kinetic characterization of Ala88 mutants of TdcD revealed the importance of this residue in determining substrate specificity. The kinetic parameters obtained for A88V TdcD were comparable to those of *M. thermophila* acetate kinase with acetate as a substrate. However, apart from Ala88, a few other residues including Arg86, Pro116, Leu117, His118 and Asp143 defining the active-site pocket also contribute to substrate specificity.

The structures of ligand-bound A88G and A88V were very similar to that of ligand-bound *St*TdcD. However, differences in the positioning of the β- and γ-phosphate

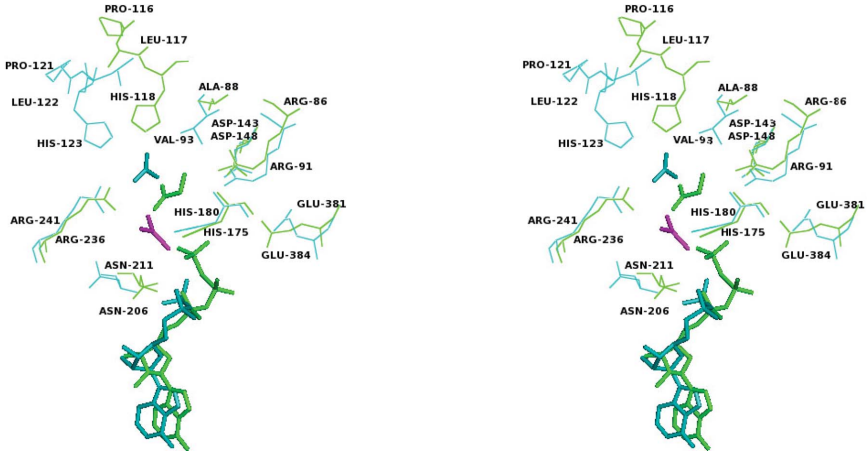

Figure 4
Stereo diagram of structural superposition of the active-site pocket of the *St*TdcD–propionate–AMPPNP complex (green) upon monomer *B* of acetate kinase from *M. thermophila* (teal). AMPPNP (green), propionate (green), acetate (teal), ADP (teal) and the transition-state analogue AlF_3 (magenta) are shown as ball-and-stick representations.

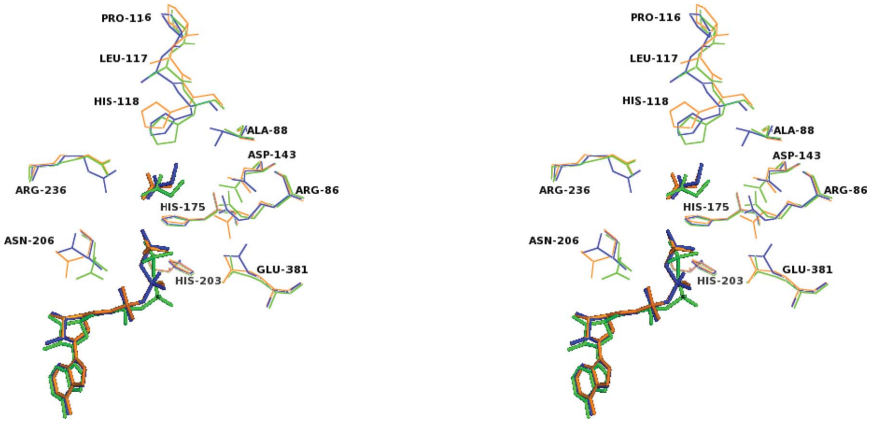

Figure 5
Stereo diagram of structural superposition of ternary complexes of Ala88G *St*TdcD (orange) and Ala88V *St*TdcD (blue) on *St*Tdc–propionate–AMPPNP (green). Ligands are shown in ball-and-stick representation.

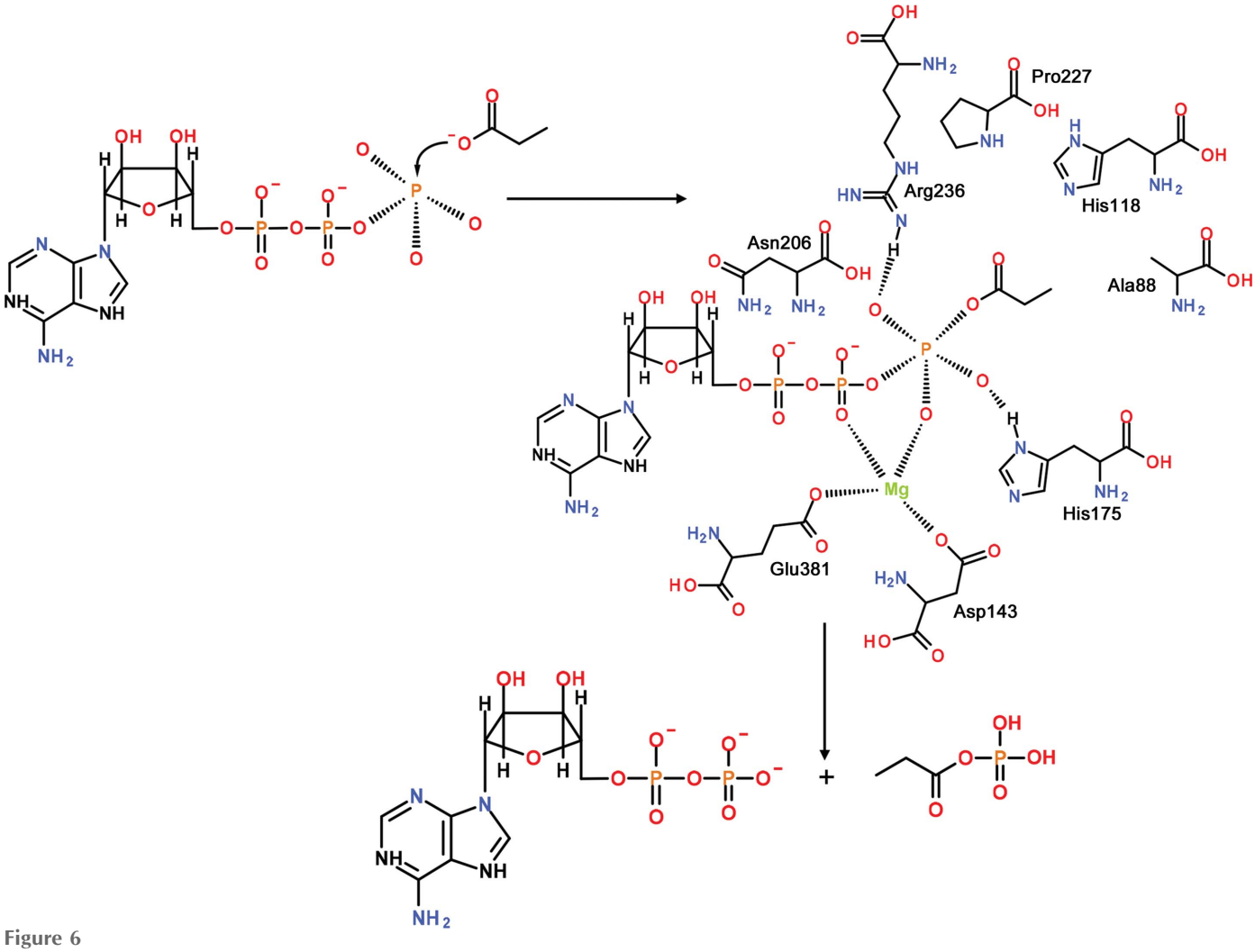

Figure 6
The proposed catalytic mechanism of propionate kinase from *S. typhimurium*.

moieties and displacement of the His118, Arg86 and Asp143 residues and the Pro116-Leu117-His118 segment were observed in the mutants (Fig. 5). The A88V and A88G mutants have a higher affinity for acetate and butyrate, respectively. These affinities are consistent with the movement of residues that is observed, where a reduction in the pocket volume of ∼30 Å^3 was observed for an increase of one methyl group in the side chain of the residue corresponding to the Ala88 position.

Based on the ligand-bound crystal structures of wild-type and mutant propionate kinases, and the transition-state analogue of acetate kinase from *M. thermophila*, a probable catalytic mechanism has been proposed (Fig. 6). In the presence of the ligand, the β-phosphate of the nucleotide is displaced towards Gly325, positioning the γ-phosphate close to the substrate. The carboxyl group of the propionate is at a distance of 4–5 Å from the γ-phosphate of the nucleotide, a distance that is suitable for the transfer of a phosphate group from the nucleotide to the substrate, suggesting direct in-line transfer. The carboxyl group of the propionate might launch a nucleophilic attack on the phosphorus, forming a penta-coordinate bipyramidal transition state. The transition state might be stabilized by the magnesium ion, Arg236 and His175 of helix α_6. Phosphoryl transfer by an associative S_N2 mechanism ensures the observed inversion of configuration. Arg86 is involved in determining the volume of the binding pocket, as its NH_2 group is at a distance of 4 Å from the propionate. The plane containing the O atoms of the transition state is perpendicular to the γ-phosphate and the phosphate group of propionyl phosphate that would be formed upon phosphoryl transfer, as required for direct in-line transfer (Schlichting & Reinstein, 1999).

5. Conclusions

The results presented in this manuscript augment structural and mechanistic understanding of propionate kinase, which plays a major role in SCFA metabolism. The crystal structures of *St*TdcD and its mutants with propionate and AMPPNP bound in the active site support an associative S_N2-type direct in-line transfer mechanism. Arg236 and His175 are catalytically important residues. Ala88 has a major role in specificity determination, along with the active-site volume-determining residues, Arg86, His118, Asp143 and the segment Pro116-

Leu117-His118. The catalytic mechanism proposed in this study may also be applicable to other acetokinase family members.

Acknowledgements

We thank the Department of Biotechnology (DBT) and the Department of Science and Technology (DST), Government of India for financial support. MRNM and HSS gratefully acknowledge J. C. Bose fellowships.

References

Bennett, W. S. Jr & Steitz, T. A. (1978). *Proc. Natl Acad. Sci. USA*, **75**, 4848–4852.
Blankenhorn, D., Phillips, J. & Slonczewski, J. L. (1999). *J. Bacteriol.* **181**, 2209–2216.
Blättler, W. A. & Knowles, J. R. (1979). *Biochemistry*, **18**, 3927–3933.
Bork, P., Sander, C. & Valencia, A. (1992). *Proc. Natl Acad. Sci. USA*, **89**, 7290–7294.
Bradford, M. M. (1976). *Anal. Biochem.* **72**, 248–254.
Buss, K. A., Cooper, D. R., Ingram-Smith, C., Ferry, J. G., Sanders, D. A. & Hasson, M. S. (2001). *J. Bacteriol.* **183**, 680–686.
Chittori, S., Savithri, H. S. & Murthy, M. R. N. (2011). *Acta Cryst.* F**67**, 1658–1661.
Chittori, S., Savithri, H. S. & Murthy, M. R. N. (2012). *BMC Struct. Biol.* **12**, 24.
Chittori, S., Simanshu, D. K., Banerjee, S., Murthy, A. M. V., Mathivanan, S., Savithri, H. S. & Murthy, M. R. N. (2013). *Biochim. Biophys. Acta*, **1834**, 2036–2044.
Cummings, J. H. & Macfarlane, G. T. (1991). *J. Appl. Bacteriol.* **70**, 443–459.
Cummings, J. H., Pomare, E. W., Branch, W. J., Naylor, C. P. & Macfarlane, G. T. (1987). *Gut*, **28**, 1221–1227.
Diao, J. & Hasson, M. S. (2009). *J. Bacteriol.* **191**, 2521–2529.
Emsley, P. & Cowtan, K. (2004). *Acta Cryst.* D**60**, 2126–2132.
Ent, F. van den, Møller-Jensen, J., Amos, L. A., Gerdes, K. & Löwe, J. (2002). *EMBO J.* **21**, 6935–6943.
Fox, D. K. & Roseman, S. (1986). *J. Biol. Chem.* **261**, 13487–13497.
Gorrell, A. & Ferry, J. G. (2007). *Biochemistry*, **46**, 14170–14176.
Gorrell, A., Lawrence, S. H. & Ferry, J. G. (2005). *J. Biol. Chem.* **280**, 10731–10742.
Hesslinger, C., Fairhurst, S. A. & Sawers, G. (1998). *Mol. Microbiol.* **27**, 477–492.
Horswill, A. R. & Escalante-Semerena, J. C. (1999). *J. Bacteriol.* **181**, 5615–5623.
Hurley, J. H. (1996). *Annu. Rev. Biophys. Biomol. Struct.* **25**, 137–162.
Kabara, J. J. & Eklund, T. (1991). *Food Preservatives*, edited by N. J. Russell & G. W. Gould, pp. 200–214. Glasgow: Blackie.
Klein, K., Steinberg, R., Fiethen, B. & Overath, P. (1971). *Eur. J. Biochem.* **19**, 442–450.
McCoy, A. J., Grosse-Kunstleve, R. W., Adams, P. D., Winn, M. D., Storoni, L. C. & Read, R. J. (2007). *J. Appl. Cryst.* **40**, 658–674.
Murshudov, G. N., Skubák, P., Lebedev, A. A., Pannu, N. S., Steiner, R. A., Nicholls, R. A., Winn, M. D., Long, F. & Vagin, A. A. (2011). *Acta Cryst.* D**67**, 355–367.
Salmond, C. V., Kroll, R. G. & Booth, I. R. (1984). *J. Gen. Microbiol.* **130**, 2845–2850.
Sawers, G. (1998). *Arch. Microbiol.* **171**, 1–5.
Sawers, G. (2001). *Mol. Microbiol.* **39**, 1285–1298.
Schlichting, I. & Reinstein, J. (1999). *Nature Struct. Biol.* **6**, 721–723.
Schnick, C., Polley, S. D., Fivelman, Q. L., Ranford-Cartwright, L. C., Wilkinson, S. R., Brannigan, J. A., Wilkinson, A. J. & Baker, D. A. (2009). *Mol. Microbiol.* **71**, 533–545.
Sears, C. L. (2005). *Anaerobe*, **11**, 247–251.
Simanshu, D. K., Chittori, S., Savithri, H. S. & Murthy, M. R. N. (2007). *J. Biosci.* **32**, 1195–1206.
Simanshu, D. K., Satheshkumar, P. S., Savithri, H. S. & Murthy, M. R. N. (2003). *Biochem. Biophys. Res. Commun.* **311**, 193–201.
Simanshu, D. K., Savithri, H. S. & Murthy, M. R. N. (2005). *J. Mol. Biol.* **352**, 876–892.
Simanshu, D. K., Savithri, H. S. & Murthy, M. R. N. (2008). *Proteins*, **70**, 1379–1388.
Spector, L. B. (1980). *Proc. Natl Acad. Sci. USA*, **77**, 2626–2630.
Weiner, M. P. & Costa, G. L. (1994). *Genome Res.* **4**, S131–S136.
Winn, M. D. *et al.* (2011). *Acta Cryst.* D**67**, 235–242.